Desalination and Water Treatment
www.deswater.com
doi: 10.5004/dwt.2020.26504

208 (2020) 287–302
December

Influence of sodium dodecyl sulfate on the morphology and performance of titanate nanotubes/polyethersulfone mixed-matrix membranes

Sylwia Mozia[a,*], Adam Czyżewski[a], Paulina Sienkiewicz[a], Dominika Darowna[a], Kacper Szymański[a,*], Michał Zgrzebnicki[b]

[a]*Department of Inorganic Chemical Technology and Environment Engineering, Faculty of Chemical Technology and Engineering, West Pomeranian University of Technology in Szczecin, Pułaskiego 10, 70-322 Szczecin, Poland, Tel. +48 91 449 47 30; emails: sylwia.mozia@zut.edu.pl (S. Mozia), kacper.szymanski@zut.edu.pl (K. Szymański), adam.czyzewski@zut.edu.pl (A. Czyżewski), paulina.sienkiewicz@zut.edu.pl (P. Sienkiewicz), ddarowna@zut.edu.pl (D. Darowna)*
[b]*Department of Catalytic and Sorbent Materials Engineering, Faculty of Chemical Technology and Engineering, West Pomeranian University of Technology in Szczecin, Pułaskiego 10, 70-322 Szczecin, Poland, email: michal.zgrzebnicki@zut.edu.pl (M. Zgrzebnicki)*

Received 19 February 2020; Accepted 25 August 2020

ABSTRACT

The influence of sodium dodecyl sulfate (SDS) on the morphology and performance of mixed-matrix polyethersulfone (PES) membranes modified with titanate nanotubes (TNTs) was studied. The membranes were prepared via wet-phase inversion method using *N,N*-dimethylformamide (DMF) as PES (15 wt.%) solvent and SDS surfactant (0.25–5 wt.%) as a hydrophilic pore forming additive. The physicochemical properties, morphology and topography of the membranes were examined on a basis of scanning electron microscopy (SEM), atomic force microscopy and contact angle measurements. The effect of casting dope composition on water permeability, rejection characteristics and resistance to fouling of the membranes was also evaluated. The SDS loading significantly influenced all the above parameters. The water permeability was correlated with the hydrophilicity and the mean size of the pores on the membrane surface. The highest pure water flux was observed for the membrane modified with 2.5 wt.% SDS and 1 wt.% (vs. PES) of TNTs. All the hybrid membranes exhibited superior antifouling properties towards bovine serum albumin (BSA) and sodium alginate (SA) compared with the neat PES one. Moreover, the fouling by SA was found to be less significant than by BSA.

Keywords: Membrane; Titanate nanotube; Sodium dodecyl sulfate; Polyethersulfone; Fouling

1. Introduction

Ultrafiltration (UF) has been recognized as an effective method suitable for numerous applications, including water and wastewater treatment [1,2], food processing [3], dairy industry [4], medicine, pharmaceutical industry [5], gas purification [6], biotechnology industry [7], paper and pulp industry [8] and others. The utilization of UF process in such extended range of applications is possible due to the development of more and more efficient membranes.

A majority of commercially available polymeric UF membranes are being manufactured via phase inversion technique, by using different types of polymers, such as polyvinylidene fluoride (PVDF) [9], cellulose acetate (CA) [10], polyacrylonitrile (PAN) [11], polysulfone (PS) [12], polyethersulfone (PES) [13], polyvinyl chloride (PVC) [14] or polypropylene (PP) [15]. Among these materials, PES is considered as a suitable polymer to be used for the fabrication of UF membranes, mostly due to its exceptional chemical and mechanical resistance, high solubility

* Corresponding authors.

in many industrial solvents and good thermal stability. However, PES membranes have a major drawback, which is the inherent problem of their fouling [16], caused by the relatively high hydrophobic characteristics of the polymer. This feature results in adsorption and deposition of feed components on the membrane surface or within its pores leading to a significant decline of permeate flux over time.

In order to limit the fouling propensity of membranes, numerous modification procedures have been investigated including blending, coating, chemical- and radiation-induced grafting and others [17]. One of the recent approaches involves the modification of PES membranes with selected nanofillers, displaying hydrophilic properties. For example, Yu et al. [18] have successfully fabricated PES UF membranes containing SiO_2 nanoparticles (NPs) modified with N-halamine. They have confirmed that permeability of the mixed-matrix membranes was superior to the pure PES membrane. Moreover, the membranes showed good antifouling properties, which was attributed to the enhancement in their surface hydrophilicity. Another group [19] was also able to procure hydrophilic PES-based composite membranes by introducing ZnO NPs. The authors have observed an improvement in flux and rejection; however, the fouling resistance was moderate compared with the pristine membrane. It was later concluded that the limited improvement in the antifouling performance was the result of insufficient surface homogeneity of the membranes, which was caused by the ZnO agglomeration. More recently titanium or titanate nanotubes (TNTs) have gained attention as promising nanofillers that could improve the main features of polymeric membranes, that is, transport, separation and antifouling properties. TNTs are characterized not only by a well-developed porous structure and large specific surface area, but they are also highly hydrophilic nanomaterials [20,21]. However, the number of publications concerning the usage of TNTs for polymeric membranes fabrication is still very limited. Mahdi et al. [22] obtained nanocomposite TNTs/PES UF membranes with improved organic matter rejection and increased pure water flux (PWF) values. Padaki et al. [23] and Shaban et al. [24] have reported that the introduction of TNTs into the polymeric matrix resulted in improvement of water permeability, as well as separation and antifouling properties of the membranes. Other authors [25,26] stated that the incorporation of TNTs inside membrane structure might enhance the desalination performance.

A more conventional approach that aimed at improving the hydrophilic properties of the membranes is incorporation of high molecular weight organic additives, especially poly(vinyl pyrrolidone) (PVP) or poly(ethylene glycols) (PEG). Wang et al. [27] have obtained PVP/PES membranes, which were characterized by a higher water flux and lower water contact angle than the neat PES membrane. The impact of PVP addition on the hydrophilic properties of the PES membranes was also studied by Abdel-Karim et al. [28] who confirmed that apart from the observed increase of hydrophilicity, the PVP modified membranes were characterized by reduced bovine serum albumin (BSA) adsorption. The increase of hydrophilicity of the PES-based membranes was also reported by Li et al. [29] after introducing to the casting solutions two different PEGs with molecular weight of 200 and 600 Da. Some research groups have also reported an increase of PES membranes hydrophilicity after introducing different surfactants into the casting dope. Amirilargani et al. [30] studied the effects of Tween 80 as an additive on the morphology and performance of flat-sheet PES membranes and found that an increase of the surfactant concentration increases hydrophilicity of the membranes. An improvement of PES membrane hydrophilicity was also reported by Ghaemi et al. [31] after introducing sodium dodecyl sulfate (SDS) directly into the dope solution for preparation of SDS/CA nanofiltration membranes. Even a small dose of SDS (0.05–0.45 wt.%) caused significant changes in membrane surface and cross-section appearance, hence considerably influencing PWF and rejection. The SDS/PAN membranes modified with functionalized multi-walled carbon nanotubes were prepared by Dastbaz et al. [32]. The authors observed enhancement of hydrophilicity, PWF and BSA rejection.

Inorganic nanofillers are known to display weak interfacial interactions with polymers such as PES [33–35], which limits their dispersion and distribution in the polymeric matrix. The inorganic NPs are also poorly dispersible in organic solvents such as dimethyl sulfoxide (DMSO), *N*,*N*-dimethylacetamide (DMAc), *N*,*N*-dimethylformamide (DMF) and *N*-methyl-2-pyrrolidone (NMP), which tends to cause their aggregation [36–40]. In terms of the mixed-matrix membrane preparation, the strong agglomeration/aggregation tendency of a nanosized filler often results in the decrease of mechanical properties and the performance of the modified membrane [34,35,41]. In view of the above, the present work is aimed at the possibility of reducing the agglomeration of TNTs and simultaneously improving the hydrophilicity of PES membrane by the application of SDS, acting as a hydrophilic, pore forming and, additionally, TNTs dispersing agent. The antiaggregating properties of SDS have been confirmed in several studies by providing sufficient dispersion stability of various NPs [42–44]. The interaction mechanism between the NPs and the surfactant has not been clearly recognized. However, it is postulated that the process is governed by steric/electrostatic repulsions and involves the adsorption of SDS hydrophilic groups on the NPs surface and the formation of a "separative layer" around the NPs, created by the SDS hydrophobic tails directed outwards [44,45].

According to the best of our knowledge, there has been no prior study on the fabrication of PES UF membranes with improved hydrophilicity and antifouling resistance by the co-incorporation of two various hydrophilic additives such as sodium dodecyl sulfate and TNTs, into the casting solution. The role of SDS as a TNTs dispersing agent capable of reducing the nanotubes agglomeration/aggregation in PES polymeric matrix was also not addressed. Therefore, the aim of this work was to investigate the effect of SDS and TNTs presence on the overall performance of the PES ultrafiltration membranes. A detailed analysis of physicochemical properties of the SDS/TNTs/PES membranes, including morphology and surface topography, hydrophilicity and water permeability was conducted. Moreover, the antifouling performance of the membranes was determined using bovine serum albumin and sodium alginate as model foulant.

2. Experimental setup

2.1. Materials

A commercially available TiO_2 (Aeroxide® P25, Evonik Industries AG, Germany), hydrochloric acid and sodium hydroxide (Avantor Performance Materials, Poland) were applied in the TNTs synthesis. Polyethersulfone (VERADEL® PESU, Solvay Plastics, Belgium), *N,N*-dimethylformamide (DMF) solvent (Avantor Performance Materials, Poland) and sodium dodecyl sulfate (SDS) surfactant (Sigma-Aldrich Chemicals, USA) were used for the preparation of membrane casting solution. Bovine serum albumin (BSA; ~66,000 g/mol; Merck, Germany) and sodium alginate (SA; 12,000–40,000 g/mol; Sigma-Aldrich Chemicals) were used as model foulants. Deionized water (type 2, 0.066 μS/cm) generated by Elix 3 (Millipore, USA) water purification system was used in all the experiments.

2.2. Preparation of TNTs

TNTs were obtained by hydrothermal treatment of TiO_2 NPs in NaOH solution according to the procedure described elsewhere [46]. 2 g of TiO_2 were dispersed in 60 mL of 10 M NaOH solution and autoclaved for 24 h at 140°C in BLH-800 pressure reactor (Berghof, Germany). The obtained slurry was washed with 0.1 M HCl solution, followed by pure water rinsing, and finally dried at 80°C for 12 h.

The transmission electron microscopy (TEM) analysis of TNTs (Fig. 1) confirmed the formation of open-ended nanotubes. The length of TNTs was in the range of 30–80 nm, while the internal and external diameter changed from 4 to 8 nm and from 9 to 10 nm, respectively.

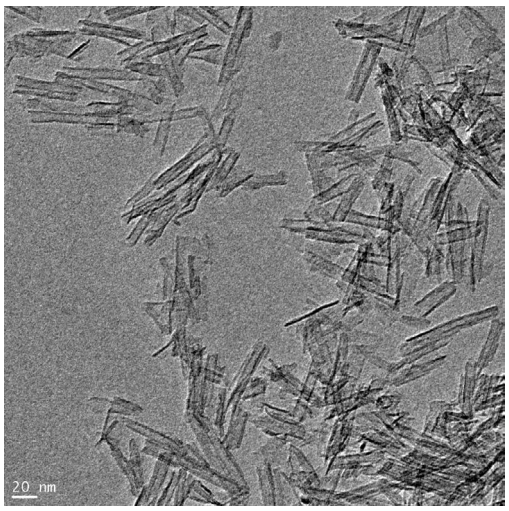

Fig. 1. TEM image of the synthesized titanate nanotubes.

2.3. Preparation of membranes

The membranes were prepared by wet-phase inversion method from casting solutions consisting of an appropriate amount of PES, DMF, SDS and TNTs (Table 1). The TNTs-loaded membranes, denoted as M6–M10, were prepared according to the following procedure. First, 1 wt.% of TNTs (by weight of PES) and an adequate amount of SDS were sonicated in 10 mL of DMF for 0.5 h by utilizing ultrasonic bath (Sonic-6D, Polsonic, Poland; output power 320 W, frequency 40 kHz). The obtained suspensions were then added into previously prepared PES/DMF solutions and magnetically stirred (at 200 rpm) for 2 h. After mixing, the casting dopes were left for degassing and subsequently casted on a glass plate using an automatic applicator (Elcometer 4340, Elcometer Ltd., UK) with a knife gap set at 0.1 mm. The casted films were immersed in deionized water coagulation bath at 20°C ± 1°C for 24 h.

The casting dopes needed for the preparation of TNTs-free membranes (M1–M5) were obtained by direct mixing (at 200 rpm) of PES, SDS and DMF. After degassing, the prepared solutions were casted using the automatic film applicator as described above.

2.4. Characterization of TNTs and membranes

The morphology of TNTs was analyzed using transmission electron microscope FEI Tecnai F20 (FEI Company, Hillsboro, USA). Prior to the analysis, the sample was dispersed in ethanol via sonication and dropped on a copper grid (300 mesh).

The cross-sectional images of the prepared membranes were acquired by utilizing Hitachi (Japan) SU8020 Ultra-High Resolution Field Emission Scanning Electron Microscope (UHR FE-SEM). Before the measurements, the membrane samples were dewatered in ethanol, fractured in liquid nitrogen, and sputter coated with chromium layer (Q150T ES, Quorum Technologies Ltd., UK). To effectively determine the structure of the membranes and the TNTs dispersion in the polymer matrix, the scanning electron microscopy (SEM) images were obtained in two modes: secondary electrons (SE; accelerating voltage 5 kV) and back-scattered electrons (BSE; accelerating voltage 15 kV).

The AFM surface images of the membranes were obtained by applying the NanoScope V Multimode 8 scanning probe microscope (Bruker Corp., USA) equipped with a silicon nitride ScanAsyst-Air probe. The measurements were conducted in the ScanAsyst mode, which uses the so-called Peak Force Tapping Mechanism. The 'Roughness' and 'Particle Analysis' functions of the NanoScope Analysis software were used, respectively, to determine the surface roughness of the membranes and size of TNT agglomerates from the images collected at the scanned area of 10 μm × 10 μm. The roughness parameter was expressed in terms of the mean roughness (R_a) values, while the size of the TNTs agglomerates was presented in a form of particle size histograms. To differentiate the aggregates and agglomerates of TNTs from the ridged surface of the polymeric matrix, the AFM technique was utilized in analysing two series of membranes. The first group included the PES membranes obtained with the addition of both SDS and TNTs, while the second group comprised of referential PES membranes prepared with the addition of SDS only. Prior to the determination of the TNTs size distribution histograms, the *z*-axis of the obtained AFM images was uniformly scaled (in the range from –150 to +150 nm) and the images were smoothed by applying the '2nd Order Flatten' function of the software. Afterwards, the uniformed AFM images were analysed by

Table 1
Composition of casting solutions

Membrane code	PES (wt.%)	SDS (wt.%)	DMF (wt.%)	TNTs (wt.% vs. PES)
M1	15	0	85	0
M2	15	0.25	84.75	0
M3	15	1	84	0
M4	15	2.5	82.5	0
M5	15	5	80	0
M6	15	0	85	1
M7	15	0.25	84.75	1
M8	15	1	84	1
M9	15	2.5	82.5	1
M10	15	5	80	1

utilizing the 'Particle Analysis' function, which provided the data used for the determination of TNTs size distribution histograms. In the cases when the obtained AFM image of the membrane surface did not allow to clearly differentiate the TNTs from the surface folds, the inconclusive image was discarded. The size of the membrane pores in the skin layer was calculated with application of the Gwyddion software package, using methodology described by Khanukaeva et al. [47] with slight modifications. Both Watershed and Threshold modes were used to define pores in the AFM images recorded at 0.5 μm × 0.5 μm scanned area.

The hydrophilic properties of the membranes were determined on the basis of the water contact angle measurements, conducted using a goniometer, model 260 (ramé-hart instruments co., USA). The static contact angle (SCA) was determined by placing a 10 μL drop of water on the surface of the membrane and measuring the angle of the drop with the substrate surface. To ensure reliable data being obtained, 10 membrane samples were measured, and the average value was reported together with the standard deviation.

2.5. Membranes performance

The performance of the prepared membranes, including PWF, BSA and SA rejection, and resistance to fouling, was determined using UF system comprised of a feed tank, a pump, a needle valve with manometer and a stainless steel membrane module.

The PWF was evaluated at the transmembrane pressure (TMP) of 0.05, 0.1 or 0.2 MPa and the feed cross-flow velocity of 0.25 m/s. The permeate flux J (L/m^{2}h) was calculated according to Eq. (1):

$$J = \frac{V}{(S \times t)} \tag{1}$$

where S represents the effective area of the membrane (0.00154 m^2), V is the permeate volume (L) and t is the time during which the permeate was collected (h).

The separation properties and fouling performances of the prepared membranes were estimated during multi-stage cross-flow filtration tests conducted by using two different feed stock solutions, containing 0.1 g/L of BSA or SA. The experiments were repeated at least four times to confirm reproducibility of the results. Before the beginning of the filtration experiment, each membrane was compacted for 1 h with deionized water under the TMP of 0.3 MPa. After the pre-compression step, the TMP was lowered to the operating pressure of 0.1 MPa, and a steady PWF ($J_{w,1}$) was recorded ("1st water stage"). The filtration experiment was continued by replacing water reservoir with BSA (or SA) feed solution, and by measuring the foulant permeate flux ($J_{f,1}$) for 1 h ("1st fouling stage"). Prior to the 2nd water-foulant filtration cycle, the fouled membrane was first subjected to alkaline cleaning, followed by pure water rinsing. Afterwards, a 2nd PWF ($J_{w,2}$) and a 2nd foulant permeate flux ($J_{f,2}$) were measured under the same condition as before. At the final stage of the filtration experiment ("3rd water stage"), the re-fouled membrane was first rinsed with pure water, and then an additional PWF ($J_{w,3}$) was recorded. The collected $J_{w,1}$, $J_{w,2}$ and $J_{w,3}$ pure water flux values were used to calculate two flux recovery ratio (FRR) parameters, expressed by Eqs. (2a) and (2b):

$$\mathrm{FRR_{NaOH}} = \left(\frac{J_{w,2}}{J_{w,1}}\right) \times 100\% \tag{2a}$$

$$\mathrm{FRR_{H_2O}} = \left(\frac{J_{w,3}}{J_{w,1}}\right) \times 100\% \tag{2b}$$

where $\mathrm{FRR_{NaOH}}$ and $\mathrm{FRR_{H_2O}}$ refer to the FRRs determined for the regenerated membrane subjected to alkaline cleaning or water rinsing, respectively.

In addition, at the end of each foulant filtration stage, the samples of permeate and retentate were collected, and the foulant rejection coefficient (R) was calculated according to Eq. (3).

$$R = \frac{C_f - C_p}{C_f} \times 100\% \tag{3}$$

where C_p and C_f are the concentration of BSA (or SA) in the permeate and feed, respectively. The concentration of

BSA and SA was determined using the total organic carbon analyzer (multi N/C 3100, Analytik Jena, Germany).

3. Results and discussion

3.1. Morphology and surface characteristics of the prepared membranes

SEM analysis was utilized to investigate the effects of SDS and TNTs addition on the morphology of the prepared membranes. The SEM images of the cross-section of all studied membranes are shown in Fig. 2.

When compared with the unmodified M1 sample, the SEM image of M6 membrane reveals no significant changes in the cross-section morphology upon addition of TNTs. Both membranes exhibited closely similar asymmetric structure comprised of a dense top layer, a porous sub-layer occupied by finger-like pores and a sponge-like structure in the bottom part of the cross-section. The only difference is the presence of TNTs agglomerate in the upper part of

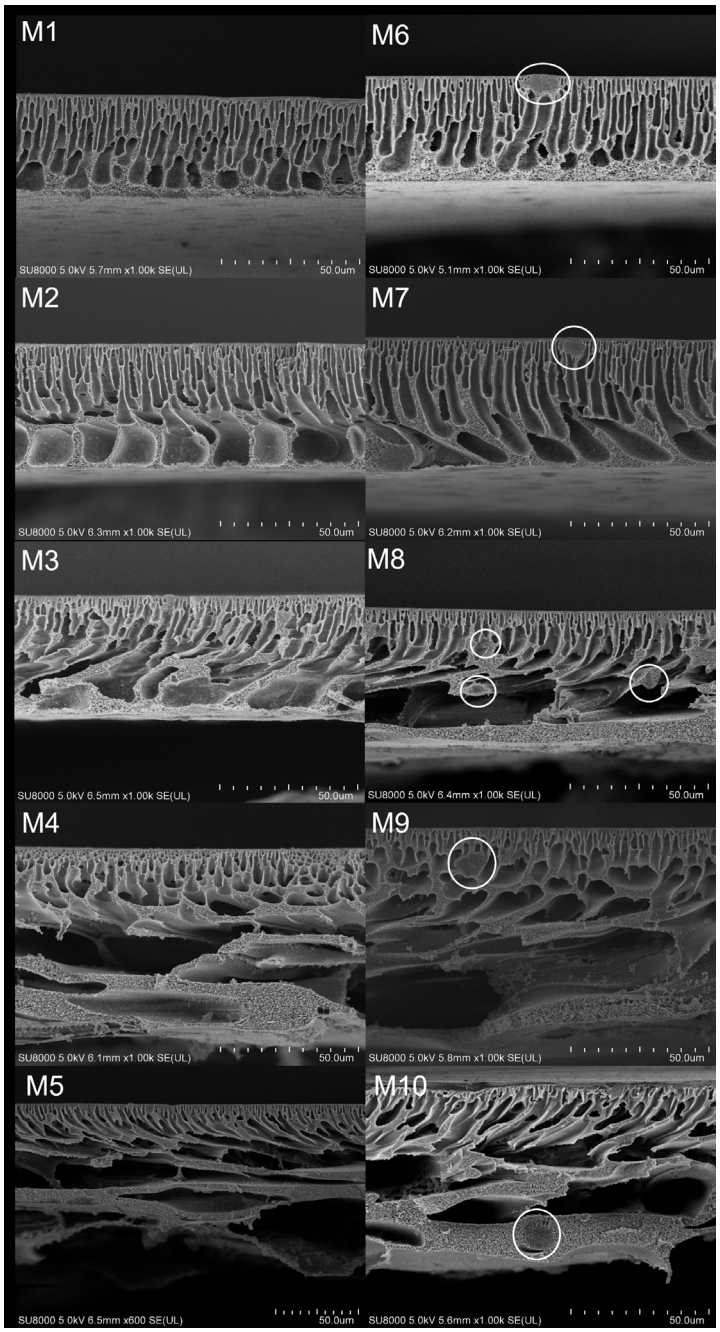

Fig. 2. SEM cross-section images of TNTs-free (M1–M5) and the corresponding TNTs-modified (M6–M10) membranes obtained with the addition of: 0 wt.% (M1, M6), 0.25 wt.% (M2, M7), 1 wt.% (M3, M8), 2.5 wt.% (M4, M9) or 5 wt.% (M5, M10) of SDS to the casting solutions.

the M6 membrane (marked with a circle). This observation coincides with the results of our previous study [48] where incorporation of different quantities of TNTs, additionally modified with silver, did not alter the overall cross-section morphology of the TNTs-loaded membranes. In case of the membranes obtained upon addition of SDS (M2–M5) or with the incorporation of SDS and TNTs (M7–M10) an increase in porosity could be observed. In general, the most significant changes were found in the sub-layer regions of the membranes and involved in the formation of irregular pores and large macrovoids. Moreover, the type and shape of the structural defects were clearly dependent on the SDS concentration. In case of the M2 and M7 membranes (obtained with the addition of 0.25 wt.% of SDS), the changes of the membranes morphology were the least profound. In the upper cross-section regions, both samples displayed a dense top layer, similar to that observed in the unmodified M1 membrane, while the sub-layer of the membranes was occupied by finger-like and tear-like structures. When the SDS concentration was increased up to 1 wt.%, the sub-layers of the resulting membranes (M3 and M8) were comprised of relatively regular finger-like structures localized in the upper part and large macrovoids in the bottom layers of the cross-sections. The most significant structural deformations were observed in the membranes obtained upon addition of 2.5 or 5 wt.% of SDS (M4, M8 and M5, M10 membranes, respectively). The samples displayed an asymmetric structure, containing top surface layer and finger-like narrow pores beneath it, while the lower regions of the membranes structure were severely distorted and occupied by disordered macrovoids and large cavities. The changes in membranes morphology correlated well with their thickness. It can be observed that the value of this parameter increased with increasing SDS concentration and reached 36–64 μm for M1–M5, and 39–66 μm for M6–M10, respectively. The mechanism governing the changes in membranes morphology in the presence of a surfactant is not fully understood; however, it could be related to the affinity between polymer and surfactant, or polymer solvent and surfactant [49]. The molecules of PES and SDS could possibly create a micelle-like complex, which reduces the interaction between the polymer chains. Moreover, amphiphilic SDS dissolved in hydrophilic DMF can create a layer of surfactant molecules on the top of the casted film, thus affecting the solvent evaporation. Both phenomena can delay the coagulation of PES, and as a result, the formation of skin layer is suppressed, while creation of finger-like pores in the support layer is enhanced. Furthermore, when the loading of SDS is relatively high, not all surfactant molecules create the PES–SDS complex. Some of them are able to form free micelles inside casting dope. These free micelles can be responsible for the deformation of pores leading to creation of defects in the membrane structure. Some of the free micelles can be located in polymer chain or can occupy any position in the membrane structure. During the coagulation in non-solvent (water), they can leave the polymer chain causing formation of the large macrovoids inside membrane structure [49–52].

Aside from the changes in the morphology of the polymeric matrix, the cross-sectional SEM images (Fig. 2) of the TNTs-modified membranes (M6–M10) confirmed the presence of TNTs agglomerates (marked by the white circles). The analysis of the size of the agglomerates revealed that the clusters in the M6 membrane (obtained without the addition of SDS) were relatively larger (mean diameter of ca. 8.7(3.5) mm) than the agglomerates located inside M7 (5.7(3.1) mm) and M8 (3.3(1.3) mm) membranes (i.e., containing 0.25 and 1 wt.% of SDS, respectively). In case of the membranes obtained using higher SDS content, the mean diameter of TNT agglomerates was larger compared with that observed for 1 wt.% of SDS and reached 4.8(2.9) mm for M9 and 6.0(2.8) mm for M10. Nevertheless, the values of standard deviation given in the brackets show that the size of the agglomerates was not uniform regardless of the SDS content. Based on the obtained results, it can be concluded that the increase of SDS amount above 1 wt.% results in re-aggregation of TNTs, as the smallest agglomerates were found in case of M8 membrane. The reduction in TNT agglomerate size in case of the membranes obtained at low SDS loading can be attributed to the positive effect of the surfactant on dispersion of NPs. Surfactants form coatings around the NPs, which due to electrostatic or steric repulsions can counterbalance van der Waals attraction forces between NPs thus preventing from their agglomeration [53]. Furthermore, the observed re-agglomeration of the NPs in the membranes obtained with the addition of higher amounts of SDS might be connected with the NPs charge neutralization phenomenon, as described by Loosli and Stoll [54]. The authors have studied the role of SDS concentration on the stability and behavior of NPs using engineered TiO_2 as model particles. They observed that at low or intermediate SDS concentrations, NPs stability is maintained and governed by the subtle interplay of SDS adsorption and acid–base properties of TiO_2 surface groups. However, at higher SDS concentration, the positive surface charge of the TiO_2 NPs was counterbalanced by the SDS negative charge, resulting in the formation of large (1,200 nm) agglomerates. It was also stated that the formation of NP clusters can be partially triggered by the occurrence of the so-called "hydrophobic effect" from the hydrocarbon tail of SDS. It was observed that owing to the hydrophobic interaction between surfactant hydrocarbon tails, a bilayer of SDS molecules could envelop the TiO_2 NPs, and thus destabilize the suspension [54].

Additional information regarding the membrane structure and the size of TNTs agglomerates was obtained by analyzing the AFM surface images of the membranes (Fig. 3). To improve the accuracy of the measurement of TNTs particles size, five different AFM surface images of the individual membranes were analyzed, and the collected data were set out in the form of particle size histograms (Fig. 4). It can be seen (Fig. 3) that the surface of the membranes without addition of TNTs was smoother than that of the samples containing NPs, however, M2–M5 samples exhibited uneven structure comprised of hills and valleys. Such corrugated surface was a result of SDS presence in the casting dope and correlated well with its content. The addition of TNTs to the casting solution resulted in the formation of their aggregates and agglomerates on the membranes surface. The histogram (Fig. 4) of M6 membrane shows the presence of relatively small (ca. 0.2 μm) as well as large (up to ca. 5 μm) TNT agglomerates. In case of histograms of M7 and M8 membranes, it can be noted that

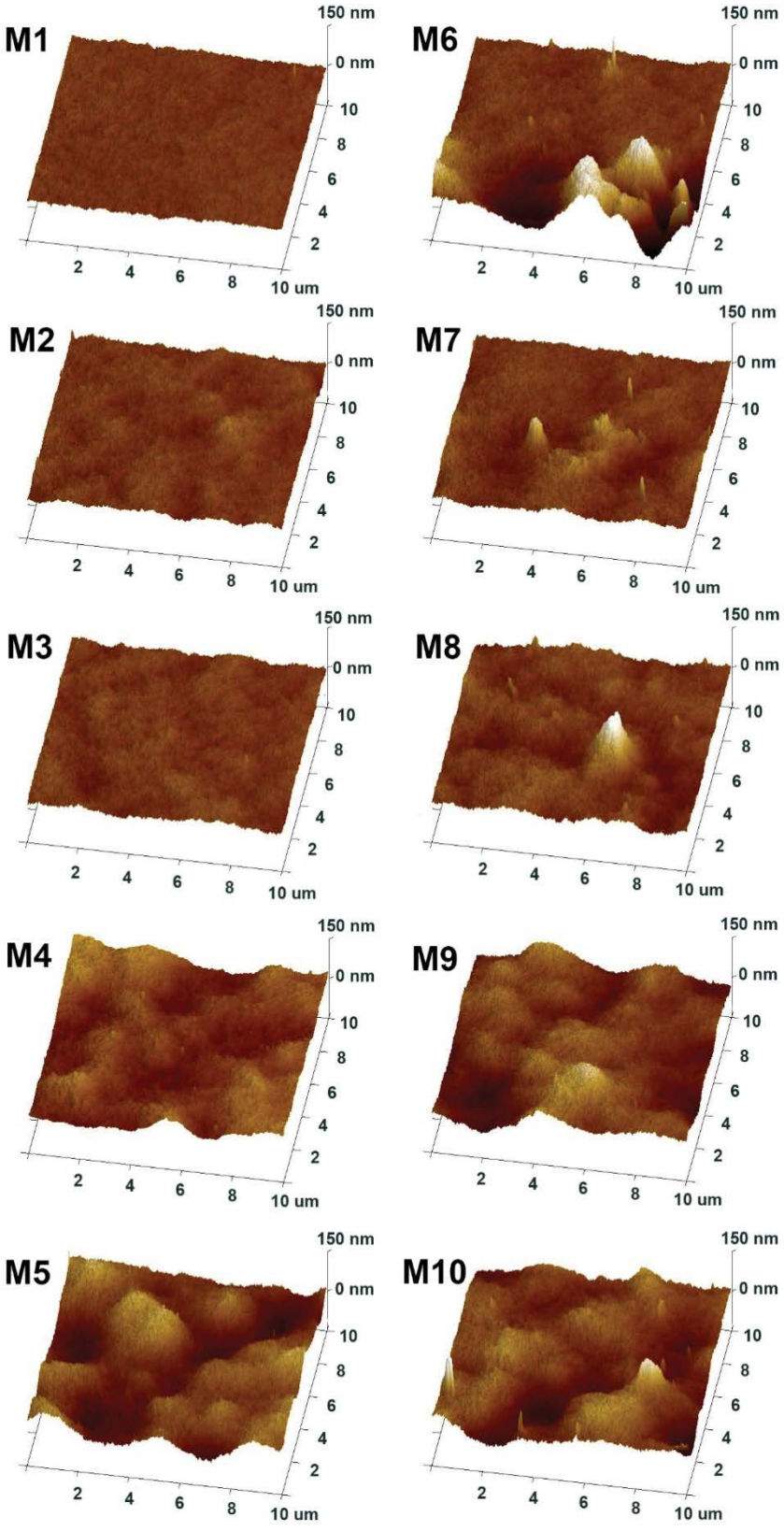

Fig. 3. AFM images of the surface (skin layer) of the TNTs-free (M1–M5) and TNTs-modified (M6–M10) membranes.

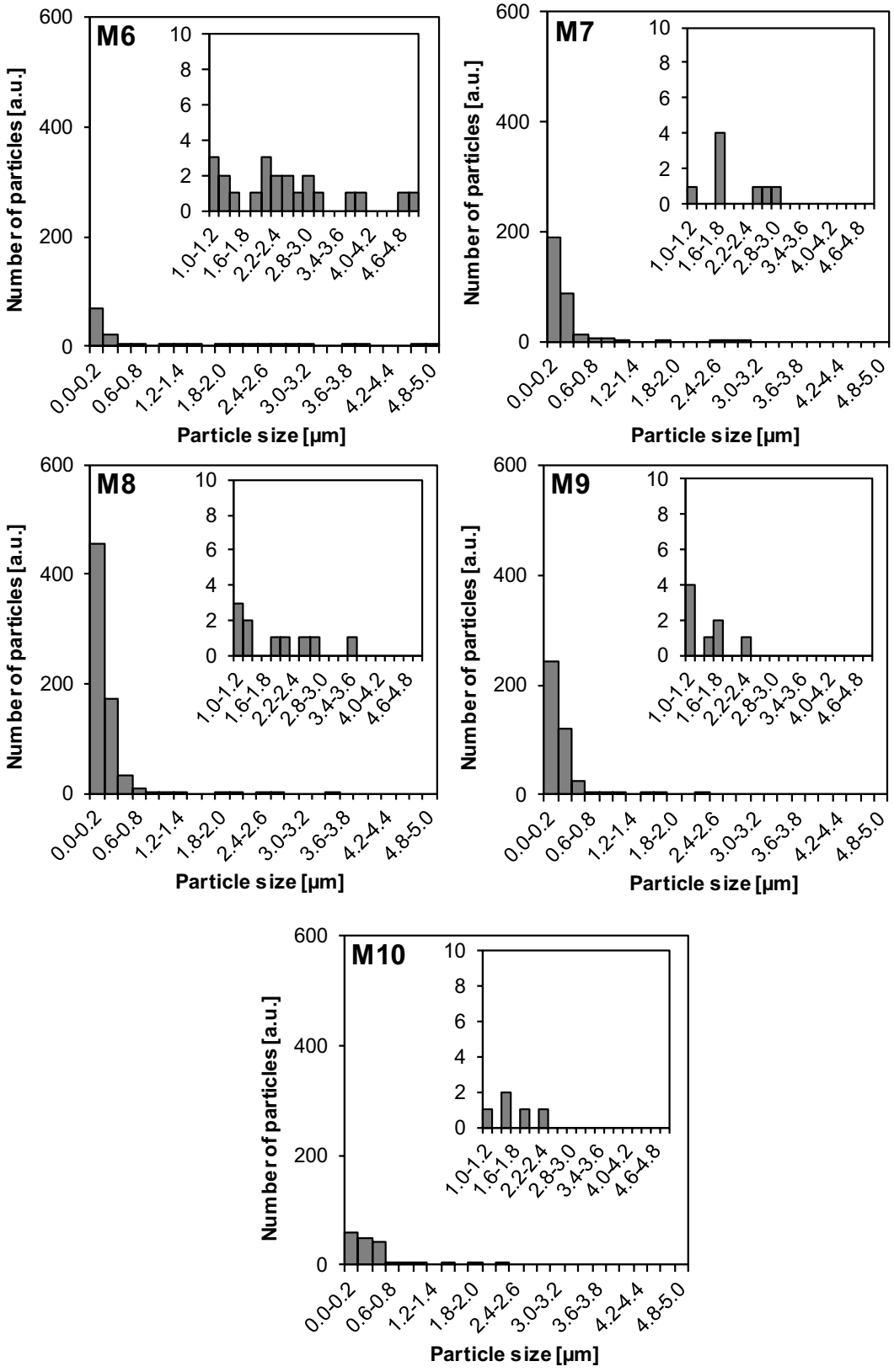

Fig. 4. Size distribution histograms of TNTs on the membrane surface.

the addition of SDS caused the larger agglomerates (above ca. 3.6 μm) to disappear, while more small agglomerates occurred. However, the histograms of M9 and M10 membranes show significant decrease of the number of smaller particles, which could indicate that the addition of higher amounts of the surfactant caused the TNT agglomerates to be placed below the membrane surface, not in/on the skin layer. One reason for that can be enhanced agglomeration of TNTs under higher SDS content (2.5 and 5 wt.%). These observations are in agreement with SEM analysis discussed above, showing that the M9 and M10 membranes were characterized by increasing diameters of TNT agglomerates observed in the cross sections compared with M8.

The heterogeneity of the topography of the membrane surface is also reflected by the mean surface roughness (R_a) values presented in Fig. 5. The addition of SDS and TNTs strongly affected this parameter. The M1 membrane had the smoothest surface represented by the lowest average surface roughness (R_a = 4.9(0.8) nm) of all the examined membranes. With the addition of SDS, the surface appeared more and more wavy, reaching the highest R_a of 20.1(2.1) nm for the M5 membrane, containing the largest amount of SDS. The increase of surface roughness with increasing SDS content is in agreement with the literature data [49]. Similar trend could be noticed for the membranes modified with TNTs. The R_a increased with the increase of SDS amount from 7.8(1.2) nm for M7 to 20.5(1.3) nm for M10. A comparison of the R_a values calculated for the membranes with and without TNTs addition revealed that the roughness increased to the highest extent in case of the membrane without SDS (M1 vs. M6). It can be also observed that the value of standard deviation calculated for the M6 membrane (error bar in Fig. 5) was significantly higher compared with the SDS-modified membranes, indicating the presence of TNT agglomerates with non-uniform sizes (Fig. 3). The least effect of TNTs presence on surface roughness was found in case of the membranes prepared using the highest loading of the surfactant (M5 vs. M10) for which the R_a values were similar to each other (20.1(2.1) vs. 20.5(1.3) nm, respectively). This can be explained by the relatively low content of TNTs on M10 surface, as was found from the size distribution histograms (Fig. 4).

The analysis of the AFM images of the membrane surface using the Gwyddion software revealed that the SDS and TNTs addition affected also the mean pore size of the membranes (Fig. 6). Samples M1–M4 (without TNTs) exhibited the pore size in the range of 6.3–6.6 nm, while upon the addition of the highest amount of SDS, the value of the pore diameter decreased to 4.6 nm. The incorporation of TNTs contributed to an increase of mean pore size, regardless of the SDS content (Fig. 6). In case of M6–M9 membranes, the pore diameter ranged from 6.4 to 6.9 nm. Similarly, as in case of the samples without TNTs addition, the application of the highest SDS loading resulted in a decrease of the pore size of M10 membrane (5.6 nm). The formation of a dense skin layer at a high surfactant concentration was already reported in the subject literature [55]. That was explained by the increase of the casting solution viscosity caused by the introduction of the additive. The increase of viscosity diminishes the diffusion exchange rate of solvent and nonsolvent, disturbing the instantaneous demixing in the coagulation bath. As aforementioned, the evident result of this phenomenon is the formation of a denser membrane with a thicker skin layer [51,56–58]. Furthermore, the increase of the surface pore size in the presence of the nanofiller, observed in Fig. 6, can be also explained on the basis of the literature data [59,60]. The increase of porosity of the membranes top layer in the presence of NPs can be attributed to the build-up and relaxation of the interfacial stresses between polymer and nanofiller, which are formed during the precipitation

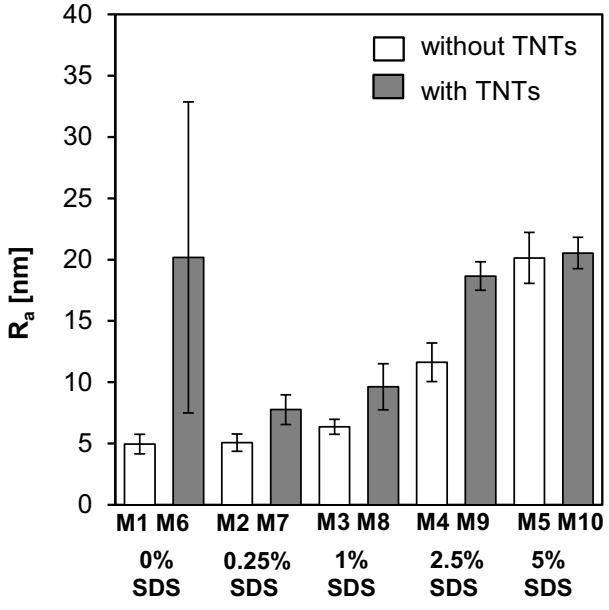

Fig. 5. Average surface roughness (R_a) of the prepared membranes.

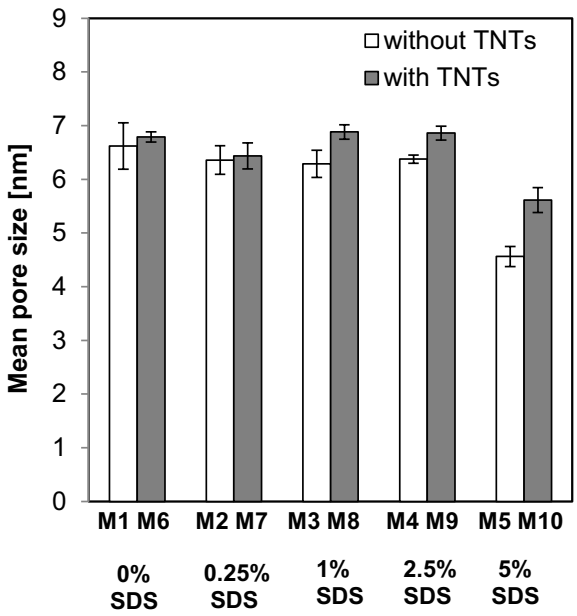

Fig. 6. Mean size of the pores present on the surface of the examined membranes.

process when shrinkage of the organic phase (polymer) is opposed by the viscoelastic behavior of the suspension (casting dope) [59].

The applied modification affected also hydrophilicity of the membranes. A more hydrophilic character can have a positive influence on the permeability and fouling resistance. As can be found from Fig. 7, both the addition of SDS as well as TNTs resulted in changes of SCA values. The increase of hydrophilicity due to the incorporation of TNTs in membranes matrix can be attributed to the presence of hydroxyl functional groups on the surface of the NPs [48]. The TNTs-modified membranes exhibited contact angle values in the range of 47°–54°. The lowest SCA was found in case of M3 and M4 membranes, while the highest for the membrane obtained without SDS addition. In case of the TNTs-free membranes, the SCA decreased from 58° for M1 to 49° for M4. However, further increase of SDS concentration hindered the improvement of hydrophilicity as SCA increased from 49° for M4 to 52° for M5. The decrease of contact angle upon SDS addition can be attributed to the structure of the surfactant molecule. SDS has a hydrophilic ionic group (sulfate group) and a hydrophobic alkyl chain [49]. The alkyl chain could be embedded in the polymer, but the hydrophilic group moves away from polymer chain, which could cause the increase of the hydrophilicity of the membrane surface. However, the roughness of the membrane skin layer can also have an impact on the contact angle, as the high roughness can reduce the hydrophilicity [61]. As was already discussed, the R_a increased with increasing SDS content (Fig. 5) reaching the highest value for 5 wt.% of SDS, which had an adverse effect on the improvement of membrane hydrophilicity.

3.2. Pure water flux

The influence of SDS and TNTs addition on the PWF of the prepared membranes is shown in Fig. 8. In general, it was found that, in comparison with TNTs-free membranes (M1–M5) the counterpart membranes (M6–M10) were characterized by higher PWF values. At this point, it ought to be noted that the amount of TNTs used during the membrane preparation was constant (1 wt.% vs. PES). Therefore, the observed changes in the permeability between the TNTs-loaded membranes (M6–M10) cannot be solely attributed to the nanotubes presence in the membrane matrix, but also to the introduction of the second additive, that is, SDS.

The results of the PWF measurements confirmed that the water transport properties of the membranes were generally dependent on the surfactant concentration used during the membrane preparation process. The impact of SDS addition was clearly less significant for the M2 and M7 membranes (obtained at relatively low surfactant concentration, that is, 0.25 wt.%), which displayed similar permeability to that of the SDS-free M1 and M6 membranes. The remaining membranes were characterized by more noticeable differences in water transport properties. An overall increase of the PWF values could be observed for the M3, M8 and M4, M9 membranes; however, a significant drop of the PWF was found for the M5 and M10 samples prepared at the highest SDS amount (i.e., 5 wt.%) in the casting dope.

When analyzing the role of the SDS presence on the water permeability of the membranes, it can be noted that the increase of the concentration of the surfactant caused a small increase of PWF until the SDS concentration reached 2.5 wt.%. Further addition of SDS resulted in a significant decrease of PWF indicating that the concentration of the surfactant in case of M5 an M10 became too high. The slight improvement of water transport properties could be linked with the increase of hydrophilicity of the M3, M4, M8 and M9 membranes (Fig. 7) compared with M1 and M5, which is in agreement with the literature data [31]. In turn, the deterioration of water permeability at the highest SDS content could be attributed to the

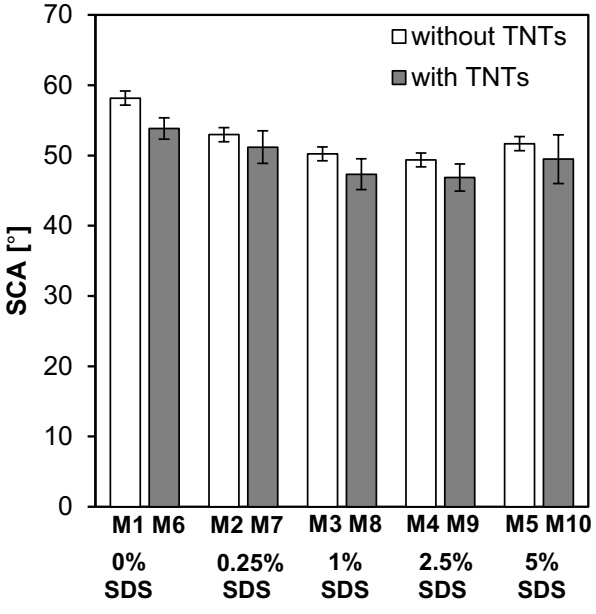

Fig. 7. Static contact angles of the prepared membranes.

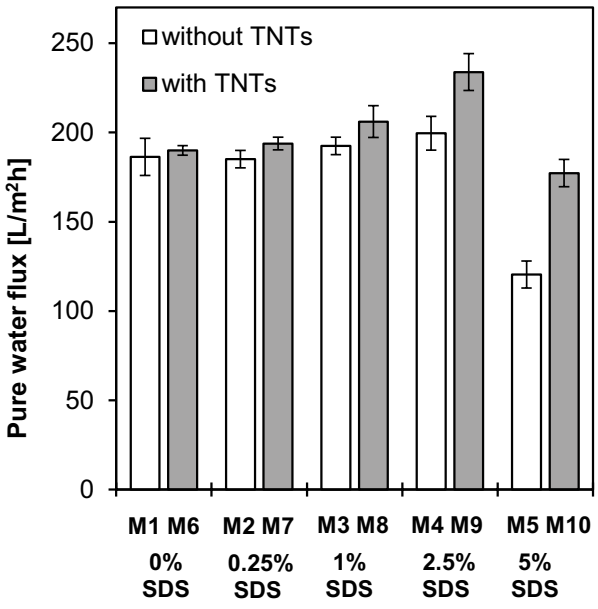

Fig. 8. Pure water flux determined for the prepared membranes. Feed: deionized water; TMP: 0.1 MPa.

decrease of hydrophilicity of the M5 and M10 membranes. These two samples were also characterized by the smallest pores (Fig. 6), which could explain their low permeability. Indeed, the analysis of the influence of the mean pore size of the membranes on PWF values (Fig. 9) revealed a good correlation between these two parameters.

3.3. Membrane fouling by BSA and SA

Fig. 10 presents a comparison of the influence of BSA and SA on membrane fouling and cleaning during ultrafiltration of model solutions at TMP = 0.1 MPa. The membranes modified with both SDS and TNTs (M7–M10) are compared with the neat M1 and the membrane modified with TNTs only (M6). It can be observed that all the mixed-matrix membranes exhibited better antifouling properties than the neat M1. Moreover, the decrease of permeate flux was less severe in case of SA compared with BSA.

The permeate flux decline during BSA filtration (Fig. 10a) was the least significant in case of the membranes obtained using 1 and 2.5 wt.% of SDS. In the 1st filtration cycle, the lowest deterioration of permeate flux was observed for M8 and M9, while the other modified membranes were significantly more prone to fouling. After 60 min of UF, the permeate flux reached the value of ca. 90 L/m^{2}h for M8 and M9, ca. 60 L/m^{2}h for M6, M7 and M10, whereas in case of the unmodified M1, it was as low as 40 L/m^{2}h. It is worth noting that simple modification of the membranes with TNTs only (M6) allowed to improve their resistance to fouling in comparison with neat M1. Nonetheless, SDS applied at a proper concentration enhanced this effect. It should be also noted that although fouling is a flux-driven phenomenon [62], the membranes characterized by the highest PWF during the initial stage (M8 and M9, Fig. 10) were less prone to fouling than the unmodified M1 exhibiting the lowest water permeability. That confirms the positive effect of the applied modification.

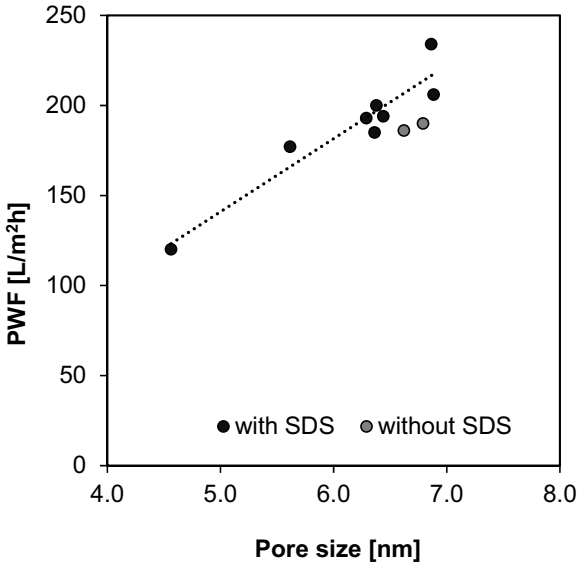

Fig. 9. The influence of mean pore diameter on PWF through the membranes. Feed: deionized water; TMP: 0.1 MPa.

In the 2nd filtration cycle, conducted after alkaline cleaning of the membranes, the lowest permeate flux was observed for neat M1 (ca. 40 L/m^{2}h); however, the differences between the fluxes measured for the mixed-matrix membranes were less apparent. At the end of this cycle, the flux ranged from about 60 to 70 L/m^{2}h. Lower permeate fluxes in the 2nd cycle compared with the 1st one can be explained in terms of membrane cleaning which was not sufficient enough to recover the initial permeability. Such an explanation is supported by the FRR values calculated after alkaline cleaning (Fig. 11a). Although in case of all the modified membranes, the efficiency of cleaning was higher compared with that observed in case of neat M1, the FRR_{NaOH} values did not exceed 95%. It is also worth noting that even though the alkaline cleaning did not allow for a complete restoration of initial permeability, its effectiveness was significantly higher compared with that of washing with water. In that case, the FRR_{H_2O} values ranged from 30% to 42%, being the lowest for M1 and the highest for M8.

In case of ultrafiltration of SA solution (Fig. 10b), the behavior of the membranes was similar to that observed for BSA. The M8 and M9 exhibited the best fouling resistance reflected by the highest permeate fluxes reaching 130 and 120 L/m^{2}h, respectively. The other mixed-matrix membranes were more prone to fouling and at the end of the 1st cycle, the fluxes ranged from ca. 80 to 90 L/m^{2}h. The most severe deterioration of permeate flux was found in case of M1 (ca. 60 L/m^{2}h after 60 min of SA filtration). In comparison with the experiment with BSA, the membrane fouling by SA was less severe what was reflected by a less steep slope of the curve representing flux decline (Fig. 10). Moreover, unlike in the presence of BSA, the changes of the permeate fluxes in the 2nd filtration cycle realized using SA solution were similar to those observed in the 1st cycle. That could be attributed to the more efficient alkaline cleaning of the membranes, as can be observed in Fig. 11b. The FRR_{NaOH} values were in the range of 96%–99% showing that the flux restoration was fairly effective even in case of the unmodified M1. On the opposite, the efficiency of washing with water was noticeably higher in case of the mixed-matrix membranes compared with M1. The FRR_{H_2O} amounted to 57% for M8 while only 37% for the neat M1 membrane. These results show a positive effect of the applied modification on the membrane fouling mitigation.

The obtained results are in agreement with literature reports showing that the incorporation of hydrophilic NPs as well as modification with SDS have a positive influence on the antifouling properties of the membranes [63]. Mokhtari et al. [63] introduced the SDS surfactant into the coagulation bath, which increased antifouling ability of polysulfone ultrafiltration membranes. Li et al. [64] showed that the incorporation of ZnO NPs into PES UF membranes caused decrease of contact angle, which resulted in better antifouling ability during filtration of BSA, SA and humic acids. The enhancement of the antifouling properties of PES UF membranes was also obtained by addition of TiO_2 [65] and TNTs [23].

The improvement of the antifouling properties of the obtained PES membranes (Figs. 10 and 11) upon the applied modification can be also related to the enhancement of their hydrophilicity. Incorporation of both TNTs and SDS

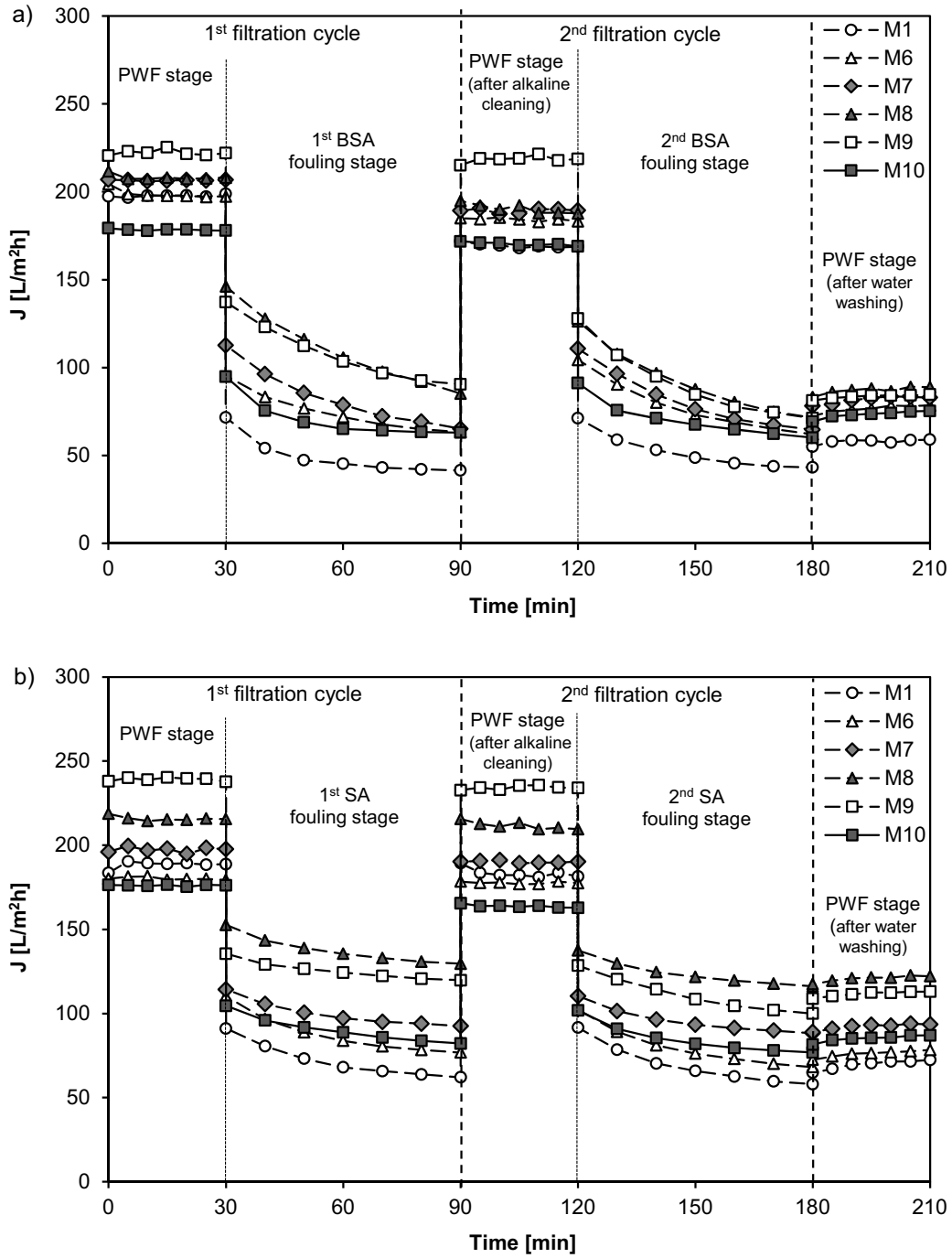

Fig. 10. Influence of BSA (a) and SA (b) on fouling of neat (M1) and modified (M6–M10) membranes. Initial concentration of foulant: 0.1 g/L. TMP = 0.1 MPa.

resulted in a decrease of contact angle of all the mixed-matrix membranes compared with the neat M1, what was discussed earlier (Fig. 7). The analysis of the influence of SCA on the decline of permeate flux after 60 min of ultrafiltration of BSA or SA solutions with reference to PWF (J_{60}/PWF) revealed that there is a clear correlation between the two parameters (Fig. 12). In other words, the more hydrophilic membrane, the higher its resistance to fouling by the organic compounds.

Furthermore, the data presented in Fig. 12 clearly show that BSA contributed to a more severe membrane fouling than SA. These differences can be attributed to the various chemical properties of these compounds. SA is considered to be more hydrophilic than BSA [66], therefore, it will be adsorbed to a lesser extent on the surface of the modified membranes, displaying a more hydrophilic characteristic (Fig. 7). Due to the relatively hydrophilic properties of both the SA molecules and membrane, the resulting repulsive

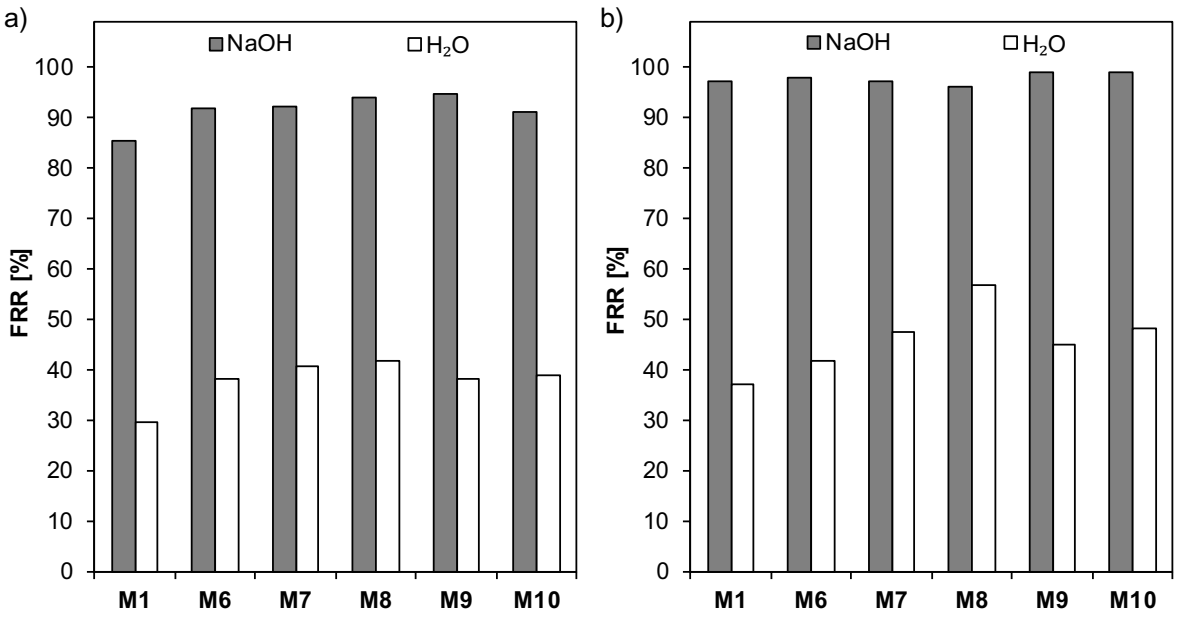

Fig. 11. Flux recovery ratio values calculated after alkaline cleaning (FRR_{NaOH}) and washing with water (FRR_{H_2O}) during ultrafiltration of: (a) BSA and (b) SA.

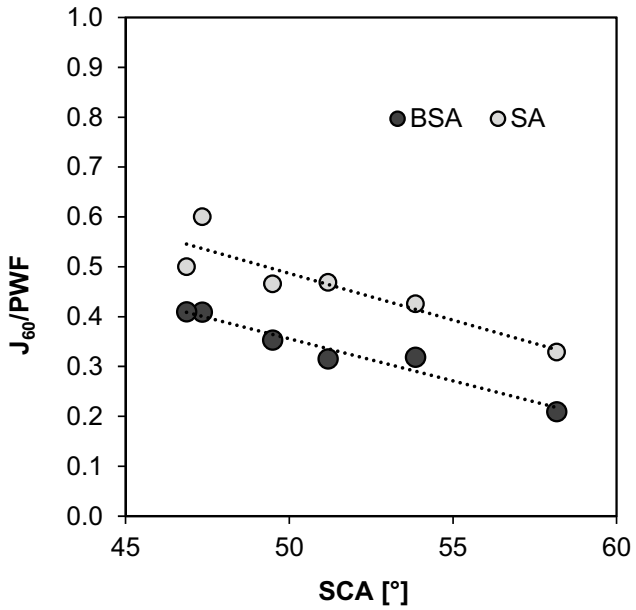

Fig. 12. Influence of membrane hydrophilicity on the decline of permeate flux after 60 min of ultrafiltration of BSA and SA solutions. Initial concentration of foulant: 0.1 g/L. TMP = 0.1 MPa.

forces between SA-SA and SA-membrane can influence the stability and cohesion of the SA fouling layer formed on the membrane surface. This trait might also explain the aforementioned differences in the FRR values observed during alkaline cleaning and water rinsing (Fig. 11) of the BSA and SA-fouled membranes. In contrast to SA, the applied cleaning and washing procedures after BSA exposure revealed the irreversible changes of permeability of the membranes. This would imply that BSA molecules are more strongly bound with the membranes, thus permanently impairing their permeation properties. Membrane fouling caused by proteins has been widely investigated over years [67–72]. The main steps of this phenomenon include (i) protein adsorption on a membrane surface, and (ii) formation of a gel-like deposit of denatured and aggregated protein on the membrane surface [72]. It was reported that an electrical repulsion between BSA and the membrane surface does not prevent from the adsorption, which indicates that this phenomenon is very complex and affected by various interactions between the membrane surface and the protein as well as between protein molecules, including van der Waals, hydrophobic, hydrophilic, structural, and steric ones [67,68]. Furthermore, proteins can expose their hydrophobic core to the surface, which makes the adsorption sensitive to hydration of protein and membrane. An important factor is also change in the shape of BSA molecules upon adsorption [68]. The presence of the exposed hydrophobic section makes the BSA molecules prone to self-aggregation, which phenomenon is known to accelerate membrane fouling by proteins [70–72].

4. Conclusions

A series of mixed-matrix PES membranes modified with TNTs and SDS were prepared by wet-phase inversion method. The morphology of the membranes was strongly affected by the concentration of SDS in the casting dope. The increase of the surfactant amount led to a formation of larger macrovoids and distorted cross-section resulting in the increase of membrane thickness and surface roughness. The concentration of SDS had also a significant influence on the size and dispersion of TNT agglomerates. The diameter of TNT agglomerates calculated on the basis of SEM analysis was the smallest in case of 1 wt.% SDS addition. At the same SDS concentration, the highest amount of

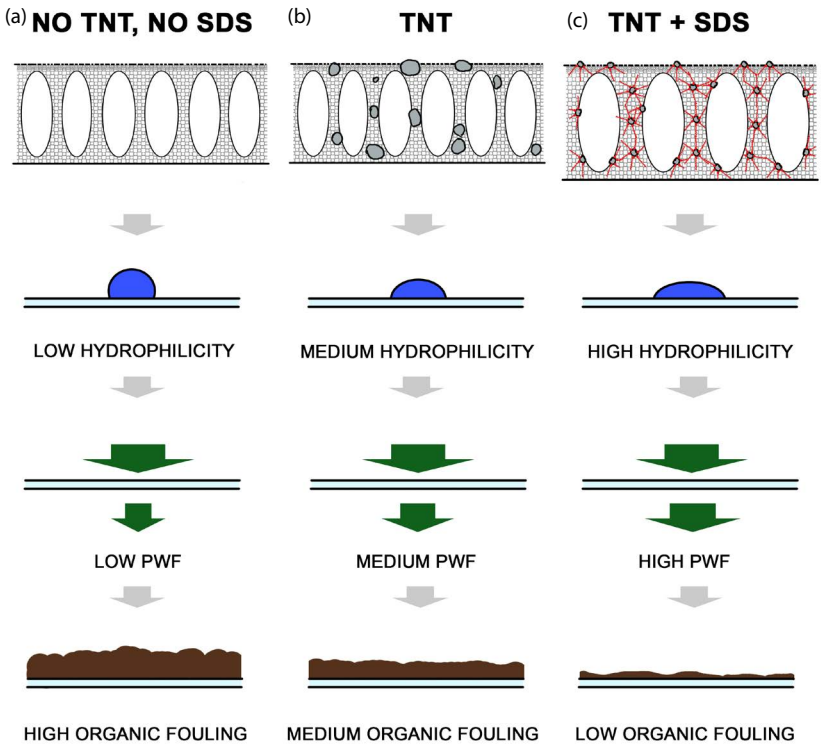

Fig. 13. Schematic diagram illustrating the influence of TNTs and/or SDS addition on the morphology, permeability and antifouling performance of the studied membranes. Commentary: (a) unmodified PES membrane revealing relatively low hydrophilicity, limited permeability and significant fouling, (b) TNTs-modified PES membrane characterized by medium hydrophilicity and improved PWF and fouling resistance, but displaying insufficient TNTs dispersion (due to NPs agglomeration), and (c) TNTs- and SDS-modified PES membranes with improved TNTs dispersion due to SDS addition, as well as enhanced permeability and superior antifouling resistance attributed to the co-incorporation of the two hydrophilic additives.

small aggregates on the membrane skin layer was observed. The improved dispersion of TNTs in the membrane matrix had a positive effect on PWF and membrane fouling mitigation. The highest water permeability and the highest resistance to fouling due to BSA and SA was observed in case of membranes prepared from casting dope containing 1 and 2.5 wt.% SDS. A correlation between the PWF values and the size of the pores in the membrane separation layer calculated on the basis of AFM images was proved. Moreover, a dependence of antifouling properties of membranes on their hydrophilicity for both SA and BSA was found. SA fouled membranes to a lesser extent than BSA and the fouling was almost completely reversible when washing with NaOH was applied. In case of rinsing with water, the FRR was lower for BSA than for SA confirming more strong interactions between the protein and the membranes compared with the polysaccharide and the membranes.

A schematic diagram summarizing the impacts of TNTs and/or SDS addition on the morphology, permeability and antifouling performance of the mixed-matrix PES membranes has been presented in Fig. 13.

Acknowledgments

This work was supported by the National Science Centre, Poland, under project No. 2016/21/B/ST8/00317.

The authors would like to thank Solvay Polska Sp. z o. o. for providing polyethersulfone samples.

Abbreviations

C_f — Concentration of BSA (or SA) in the feed
C_p — Concentration of BSA (or SA) in the permeate
DMAc — *N*,*N*-Dimethylacetamide
DMF — *N*,*N*-Dimethylformamide
FRR_{H_2O} — Flux recovery ratio determined for the regenerated membrane subjected to water rinsing
FRR_{NaOH} — Flux recovery ratio determined for the regenerated membrane subjected to alkaline cleaning
J — Permeate flux, L/m^{2}h
$J_{f,1}$ — 1st foulant permeate flux measured after 1 h of foulant filtration (1st fouling stage)
$J_{f,2}$ — 2nd foulant permeate flux measured after 1 h of foulant filtration (2nd fouling stage)
$J_{w,1}$ — 1st steady pure water flux
$J_{w,2}$ — 2nd steady pure water flux
$J_{w,3}$ — 3rd steady pure water flux
NMP — *N*-methyl-2-pyrrolidone
R — Foulant rejection coefficient
R_a — Surface roughness

S — Effective area of the membrane
t — Time, h
V — Volume, L

References

[1] G.-d. Kang, Y.-m. Cao, Application and modification of poly(vinylidene fluoride) (PVDF) membranes-a review, J. Membr. Sci., 463 (2014) 145–165.
[2] N.A. Alenazi, M.A. Hussein, K.A. Alamry, A.M. Asiri, Modified polyether-sulfone membrane: a mini review, Des. Monomers Polym., 20 (2017) 532–546.
[3] A.W. Mohammad, C.Y. Ng, Y.P. Lim, G.H. Ng, Ultrafiltration in food processing industry: review on application, membrane fouling, and fouling control, Food Bioprocess Tech., 5 (2012) 1143–1156.
[4] P. Kumar, N. Sharma, R. Ranjan, S. Kumar, Z.F. Bhat, D.K. Jeong, Perspective of membrane technology in dairy industry: a review, Asian Austral. J. Anim., 26 (2013) 1347–1358.
[5] D. Chen, K.K. Sirkar, C. Jin, D. Singh, R. Pfeffer, Membrane-based technologies in the pharmaceutical industry and continuous production of polymer-coated crystals/particles, Curr. Pharm. Design, 23 (2017) 242–249.
[6] R.S. Murali, T. Sankarshana, S. Sridhar, Air separation by polymer-based membrane technology, Sep. Purif. Rev., 42 (2013) 130–186.
[7] A. Basile, S. Mozia, R. Molinari, Current Trends and Future Developments on (Bio-) Membranes, 1st ed., Elsevier, Amsterdam, Netherlands, 2018.
[8] O. Olsen, Membrane technology in the pulp and paper industry, Desalination, 35 (1980) 291–302.
[9] V. Vatanpour, A. Ghadimi, A. Karimi, A. Khataee, M.E. Yekavalangi, Antifouling polyvinylidene fluoride ultrafiltration membrane fabricated from embedding polypyrrole coated multiwalled carbon nanotubes, Mater. Sci. Eng. C, 89 (2018) 41–51.
[10] J. Zhou, J. Chen, M. He, J. Yao, Cellulose acetate ultrafiltration membranes reinforced by cellulose nanocrystals: preparation and characterization, J. Appl. Polym. Sci., 133 (2016) 43946–43953.
[11] S. Jegan, M. Beri, J. Pramila, R. Dipak, N. Alagumalai, N. Nagarajan, G. Nagendra, R.M Doraiswamy, Customized antifouling polyacrylonitrile ultrafiltration membranes for effective removal of organic contaminants from aqueous stream, J. Chem. Technol. Biotechnol., 94 (2019) 859–868.
[12] P.T.P. Aryanti, A.M. Noviyani, M.F. Kurnia, D.A. Rahayu, A.Z. Nisa, Modified polysulfone ultrafiltration membrane for humic acid removal during peat water treatment, IOP Conf. Ser.: Mater. Sci. Eng., 288 (2018) 012118.
[13] J. Xiang, X. Hua, X. Dong, P. Cheng, L. Zhang, W. Du, N. Tang, Effect of nonsolvent additives on PES ultrafiltration membrane pore structure, J. Appl. Polym. Sci., 136 (2019) 47525–47533.
[14] B.S. Dizajikan, M. Asadollahi, S.A. Musavi, D. Bastani, Preparation of poly(vinyl chloride) (PVC) ultrafiltration membranes from PVC/additive/solvent and application of UF membranes as substrate for fabrication of reverse osmosis membranes, J. Appl. Polym. Sci., 135 (2018) 46267–46279.
[15] S. Hoseinpour, Y. Jafarzadeh, R. Yegani, S. Masoumi, Embedding neat and carboxylated nanodiamonds into polypropylene membranes to enhance antifouling properties, Polyolefins J., 6 (2019) 63–74.
[16] L.D. Tijing, Y.C. Woo, J.S. Choi, S. Lee, S.H. Kim, H.K. Shon, Fouling and its control in membrane distillation-a review, J. Membr. Sci., 475 (2015) 215–244.
[17] A. Abdelrasoul, H. Doan, A. Lohi, Fouling in Membrane Filtration and Remediation Methods, in: H. Nakajima, Mass Transfer-Advances in Sustainable Energy and Environment Oriented Numerical Modeling, IntechOpen, Open access peer-reviewed Edited Volume, 2013.
[18] H. Yu, X. Zhang, Y. Zhang, J. Liu, H. Zhang, Development of a hydrophilic PES ultrafiltration membrane containing SiO_2@N-Halamine nanoparticles with both organic antifouling and antibacterial properties, Desalination, 326 (2013) 69–76.
[19] A.L. Ahmad, J. Sugumaran, N.F. Shoparwe, Antifouling properties of PES membranes by blending with ZnO nanoparticles and NMP-acetone mixture as solvent, Membranes, 8 (2018) 131–144.
[20] W. Liu, J. Ni, X. Yin, Synergy of photocatalysis and adsorption for simultaneous removal of Cr(VI) and Cr(III) with TiO_2 and titanate nanotubes, Water Res., 53 (2014) 12–25.
[21] Q. Chen, L. Peng, Structure and applications of titanate and related nanostructures, Int. J. Nanotechnol., 4 (2007) 44–65.
[22] N. Mahdi, P. Kumar, A. Goswami, B. Perdicakis, K. Shankar, M. Sadrzadeh, Robust polymer nanocomposite membranes incorporating discrete TiO_2 nanotubes for water treatment, Nanomaterials, 9 (2019) 1186–1204.
[23] M. Padaki, D. Emadzadeh, T. Masturra, A.F. Ismail, Antifouling properties of novel PSf and TNT composite membrane and study of effect of the flow direction on membrane washing, Desalination, 362 (2015) 141–150.
[24] M. Shaban, H. Abdallah, L. Said, H.S. Hamdy, A.A. Khalek, Titanium dioxide nanotubes embedded mixed matrix PES membranes characterization and membrane performance, Chem. Eng. Res. Des., 95 (2014) 307–316.
[25] H. Abdallah, A.F. Moustafa, A.A. Al Anezi, H.E.M. El-Sayed, Performance of a newly developed titanium oxide nanotubes/polyethersulfone blend membrane for water desalination using vacuum membrane distillation, Desalination, 346 (2014) 30–36.
[26] A. Sumisha, G. Arthanareeswaran, A.F. Ismail, D.P. Kumar, M.V. Shankar, Functionalized titanate nanotube-polyetherimide nanocomposite membrane for improved salt rejection under low pressure nanofiltration, RSC Adv., 5 (2015) 39464–39473.
[27] H.T. Wang, T. Yu, C.Y. Zhao, Q.Y. Du, Improvement of hydrophilicity and blood compatibility on polyethersulfone membrane by adding polyvinylpyrrolidone, Fibers Polym., 10 (2009) 1–5.
[28] A. Abdel-Karim, T.A. Gad-Allah, A.S. El-Kalliny, S.I.A. Ahmed, E.R. Souaya, M.I. Badawy, M. Ulbricht, Fabrication of modified polyethersulfone membranes for wastewater treatment by submerged membrane bioreactor, Sep. Purif. Technol., 175 (2017) 36–46.
[29] J.-F. Li, Z.-L. Xu, H. Yang, C.-P. Feng, J.-H. Shi, Hydrophilic microporous PES membranes prepared by PES/PEG/DMAc casting solutions, J. Appl. Polym. Sci., 107 (2008) 4100–4108.
[30] M. Amirilargani, E. Saljoughi, T. Mohammadi, Effects of Tween 80 concentration as a surfactant additive on morphology and permeability of flat sheet polyethersulfone (PES) membranes, Desalination, 249 (2009) 837–842.
[31] N. Ghaemi, S.S. Madaeni A. Alizadeh, P. Daraei, V. Vatanpour, M. Falsafi, Fabrication of cellulose acetate/sodium dodecyl sulfate nanofiltration membrane: characterization and performance in rejection of pesticides, Desalination, 290 (2012) 99–106.
[32] Z. Dastbaz, M. Pakizeh, M. Namvar-Mahboub, The effect of functionalized MWCNT and SDS on the characteristic and performance of PAN ultrafiltration membrane, Desal. Water Treat., 57 (2016) 24267–24277.
[33] L. Wang, X. Song, T. Wang, S. Wang, Z. Wang, C. Gao, Fabrication and characterization of polyethersulfone/carbon nanotubes (PES/CNTs) based mixed matrix membranes (MMMs) for nanofiltration application, Appl. Surf. Sci., 330 (2015) 118–125.
[34] A. Sotto, A. Boromand, R. Zhang, P. Luis, J.M. Arsuaga, J. Kim, B. Van der Bruggen, Effect of nanoparticle aggregation at low concentrations of TiO_2 on the hydrophilicity, morphology, and fouling resistance of PES–TiO_2 membranes, J. Colloid Interface Sci., 363 (2011) 540–550.
[35] A. Sotto, A. Boromand, S. Balta, J. Kim, B. Van der Bruggen, Doping of polyethersulfone nanofiltration membranes: antifouling effect observed at ultralow concentrations of TiO_2 nanoparticles, J. Mater. Chem., 21 (2011) 10311–10320.
[36] J.H. Choi, J. Jegal, W.N. Kim, Fabrication and characterization of multi-walled carbon nanotubes/polymer blend membranes, J. Membr. Sci., 284 (2006) 406–415.
[37] M. Sianipar, S.H. Kim, C. Min, L.D. Tijing, H.K. Shon, Potential and performance of a polydopamine-coated multiwalled

carbon nanotube/polysulfone nanocomposite membrane for ultrafiltration application, J. Ind. Eng. Chem., 34 (2016) 364–373.
[38] M. Cao, Q. Liu, M. Chen, P. Yang, Y. Xu, H. Wu, J. Yu, L. He, X.H. Zhang, Q. Zhang, Dispersing hydrophilic nanoparticles in nonaqueous solvents with superior long-term stability, RSC Adv., 7 (2017) 25535–25541.
[39] V.S. Nguyen, D. Rouxel, B. Vincent, Dispersion of nanoparticles: from organic solvents to polymer solutions, Ultrason. Sonochem., 21 (2014) 149–153.
[40] S. Ghosh, A. Gomathi, C.N.R. Rao, Stable dispersions of metal oxide nanowires and nanoparticles in water, dimethylformamide and toluene, J. Nanosci. Nanotechnol., 9 (2009) 5214–5222.
[41] Z. Spitalsky, D. Tasis, K. Papagelis, C. Galiotis, Carbon nanotube–polymer composites: chemistry, processing, mechanical and electrical properties, Prog. Polym. Sci., 35 (2010) 357–401.
[42] C. Wang, Li. Ma, W. Yang, Effect of surfactants on the dispersion of multi-walled carbon nanotubes in epoxy resin, Adv. Mater. Res., 221 (2011) 1–7.
[43] L. Kvítek, A. Panáček, J. Soukupová, M. Kolář, R. Večeřová, R. Prucek, M. Holecová, R. Zbořil, Effect of surfactants and polymers on stability and antibacterial activity of silver nanoparticles (NPs), J. Phys. Chem. C, 112 (2008) 5825–5834.
[44] X. Li, Y. Qin, C. Liu, S. Jiang, L. Xiong, Q. Sun, Size-controlled starch nanoparticles prepared by self-assembly with different green surfactant: the effect of electrostatic repulsion or steric hindrance, Food Chem., 199 (2016) 356–363.
[45] S. Skoglund, T.A. Lowe, J. Hedberg, E. Blomberg, I. Odnevall Wallinder, S. Wold, M. Lundin, Effect of laundry surfactants on surface charge and colloidal stability of silver nanoparticles, Langmuir, 29 (2013) 8882–8891.
[46] T. Kasuga, Formation of titanium oxide nanotubes using chemical treatments and their characteristic properties, Thin Solid Films, 496 (2006) 141–145.
[47] D.Y. Khanukaeva, A.N. Filippov, A.V. Bildyukevich, An AFM study of ultrafiltration membranes: peculiarities of pore size distribution, Petrol. Chem., 54 (2014) 498–506.
[48] S. Mozia, P. Sienkiewicz, K. Szymański, M. Zgrzebnicki, D. Darowna, A. Czyżewski, A.W. Morawski, Influence of Ag/titanate nanotubes on physicochemical, antifouling and antimicrobial properties of mixed-matrix polyethersulfone ultrafiltration membranes, J. Chem. Technol. Biotechnol., 94 (2019) 2497–2511.
[49] A. Rahimpour, S.S. Madaeni, Y. Mansourpanah, The effect of anionic, non-ionic and cationic surfactants on morphology and performance of polyethersulfone ultrafiltration membranes for milk concentration, J. Membr. Sci., 296 (2007) 110–121.
[50] C.H. Loh, R. Wanga, L. Shib, A.G. Fane, Fabrication of high performance polyethersulfone UF hollow fiber membranes using amphiphilic Pluronic block copolymers as pore-forming additives, J. Membr. Sci., 380 (2011) 114–123.
[51] S. Saedi, S.S. Madaeni, A.A. Shamsabadi, F. Mottaghi, The effect of surfactants on the structure and performance of PES membrane for separation of carbon dioxide from methane, Sep. Purif. Technol., 99 (2012) 104–119.
[52] N. Peng, T.S. Chung, K.Y. Wang, Macrovoid evolution and critical factors to form macrovoid-free hollow fiber membranes, J. Membr. Sci., 318 (2008) 363–372.
[53] B.M. Paramashivaiah, C.R. Rajashekhar, Studies on effect of various surfactants on stable dispersion of graphene nano particles in simarouba biodiesel, IOP Conf. Ser.: Mater. Sci. Eng., 149 (2016) 012083–012093.
[54] F. Loosli, S. Stoll, Effect of surfactants, pH and water hardness on the surface properties and agglomeration behavior of engineered TiO_2 nanoparticles, Environ. Sci.: Nano, 4 (2017) 203–211.
[55] M. Omidvar, M. Soltanieh, S.M. Mousavi, E. Saljoughi, A. Moarefian, H. Saffaran, The effect of Merpol surfactant on the morphology and performance of PES/PVP membranes: antibiotic separation, Int. J. Ind. Chem., 10 (2019) 301–309.
[56] M. Liu, C. Xiao, X. Hu, Effects of non-solvent additives on PVDF solution viscosity and membrane performance, Iran. Polym. J., 20 (2011) 979–988.
[57] V. Vatanpour, S.S. Madaeni, R. Moradian, S. Zinadini, B. Astinchap, Fabrication and characterization of novel antifouling nanofiltration membrane prepared from oxidized multiwalled carbon nanotube/polyethersulfone nanocomposite, J. Membr. Sci., 375 (2011) 284–294.
[58] E. Saljoughi, S.M. Mousavi, Preparation and characterization of novel polysulfone nanofiltration membranes for removal of cadmium from contaminated water, Sep. Purif. Technol., 90 (2012) 22–30.
[59] Y. Yang, H. Zhang, P. Wang, Q. Zheng, J. Li, The influence of nano-sized TiO_2 fillers on the morphologies and properties of PSF UF membrane, J. Membr. Sci., 288 (2007) 231–238.
[60] P. Aerts, I. Genne, S. Kuypers, R. Leysen, I.F.J. Vankelecom, P.A. Jacobs, Polysulfone-aerosil composite membranes. Part 2. The influence of the addition of aerosil on the skin characteristics and membrane properties, J. Membr. Sci., 178 (2000) 1–11.
[61] K.J. Kubiak, M.C.T. Wilson, T.G. Mathia, P. Carval, Wettability versus roughness of engineering surfaces, Wear, 271 (2011) 523–528. https://doi.org/10.1016/j.wear.2010.03.029.
[62] R. Field, Chapter 1 – Fundamentals of Fouling, K.V. Peinemann, S. Pereira Nunes, Eds., Membrane Technology: Volume 4: Membranes for Water Treatment, WILEY-VCH Verlag GmbH & Co. KGaA, Weinheim, 2010.
[63] S. Mokhtari, A. Rahimpour, A.A. Shamsabadi, S. Habibzadeh, M. Soroush, Enhancing performance and surface antifouling properties of polysulfone ultrafiltration membranes with salicylate-alumoxane nanoparticles, Appl. Surf. Sci., 393 (2017) 93–102.
[64] X. Li, J. Li, B. Van der Bruggen, X. Sun, J. Shen, W. Hana, L. Wang, Fouling behavior of polyethersulfone ultrafiltration membranes functionalized with sol-gel formed ZnO nanoparticles, RSC Adv., 5 (2015) 50711–50719.
[65] X. Li, J. Li, X. Fang, K. Bakzhan, L. Wang, B. Van der Bruggen, A synergetic analysis method for antifouling behavior investigation on PES ultrafiltration membrane with self-assembled TiO_2 nanoparticles, J. Colloid Interface Sci., 469 (2016) 164–176.
[66] N. Subhi, A.R.D. Verliefde, V. Chen, P. Le-Clech, Assessment of physicochemical interactions in hollow fibre ultrafiltration membrane by contact angle analysis, J. Membr. Sci., 403–404 (2012) 32–40.
[67] A. Barroug, E. Lernoux, J. Lemaitre, P.G. Rouxhet, Adsorption of catalase on hydroxyapatite, J. Colloid Interface Sci., 208 (1998) 147–152.
[68] S. Salgin, S. Takac, T.H. Ozdamar, Adsorption of bovine serum albumin on polyether sulfone ultrafiltration membranes: determination of interfacial interaction energy and effective diffusion coefficient, J. Membr. Sci., 278 (2006) 251–260.
[69] M. Veen, W. Norde, M.C. Stuart, Electrostatic interactions in protein adsorption probed by comparing lysozyme and succinylated lysozyme, Colloid Surf., B, 35 (2004) 33–40.
[70] C. Huggins, D.F. Tapley, E.V. Jensen, Sulphydryl-disulphide relationships in the induction of gels in proteins by urea, Nature, 167 (1951) 592–593.
[71] V.M. Rosenoer, M. Oratz, M.A. Rothschild, Albumin: Structure, Function and Uses, Pergamon Press, Oxford, UK, 1977.
[72] T. Maruyama, S. Katoh, M. Nakajima, H. Nabetani, Mechanism of bovine serum albumin aggregation during ultrafiltration, Biotechnol. Bioeng., 75 (2001) 233–238.